

Title

The application of remote sensing techniques to monitor CO₂ storage sites for surface leakage: method development and testing at Latera (Italy) where naturally-produced CO₂ is leaking to the atmosphere

Authors

L. Bateson (1), M. Vellico (2), S.E. Beaubien (3), J.M. Pearce (1); A. Annunziatellis (3), G. Ciotoli (3), F. Coren (2), S. Lombardi (3), and S. Marsh (1)

Affiliations

- (1) British Geological Survey (BGS), Keyworth, UK,
- (2) Istituto Nazionale di Oceanografia e di Geofisica Sperimentale (OGS), Trieste, Italy
- (3) Dipartimento di Scienze della Terra, Università di Roma “La Sapienza” (URS), Rome, Italy,

Corresponding author

Stan Beaubien (c/o Prof. Salvatore Lombardi)
Dipartimento di Scienze della Terra
Università di Roma “La Sapienza”
Piazzale Aldo Moro, 5
00185, Rome, Italy

+39-(0)6-49914918 or +39-(0)6-49914919

stanley.beaubien@uniroma1.it

Abstract

Two airborne remote sensing flights were conducted above a geothermal field in central Italy (the LATERA caldera) where deep, naturally-produced CO₂ is migrating to surface along faults and leaking to the atmosphere at spatially-restricted gas vents. The goal of these surveys was to understand if it is possible to locate CO₂ leaking from a CO₂ geological storage site through the application of indirect remote sensing methods that primarily measure plant stress and subsequent ground-based verification using near-surface gas geochemistry techniques. The overall success rate obtained by integrating six different datasets was 39%, although some individual techniques, such as one NDVI survey, achieved a 47% success rate. While the work did discover some vents that were previously unknown, it also failed to locate 5 vents that are known to exist and, perhaps, other unknown vents. Future work will focus on understanding the various causes of false positives, automation of preliminary data interpretation, and the direct hyperspectral measurement of atmospheric CO₂ produced by these natural seeps.

Keywords: CO₂ geological storage; remote sensing; leakage monitoring; gas geochemistry verification; natural analogue

1. Introduction

The capture of CO₂ from large-scale industrial emitters and its underground storage in geological structures could help meet Kyoto and post-Kyoto commitments. Together with renewable energy production and increased energy efficiency, this may help provide a transition to the 'hydrogen economy'. The potential exists for the long-term safe storage of significant amounts of CO₂, provided that the stored CO₂ remains below ground.

Successful long-term containment of CO₂ deep underground will depend on demonstrating acceptable performance, verifying that the CO₂ remains underground, and answering operational, regulatory, and public acceptance criteria. Scientific and technological advances have been made in carbon capture, transport, and storage using demonstration and pilot studies. However, there is a lack of fundamental research concerning long-term verification, safety, and environmental issues (West et al., 2005). In particular, the effects of long-term leakage, whether slow or through catastrophic release, on terrestrial ecosystems have only recently been explored by the carbon storage research community (see for example Beaubien et al., this issue; Hepple and Benson, 2005; Lewicki et al., 2005; Lewicki and Oldenburg, 2004; Oldenburg and Lewicki, 2006; Pearce and West, 2006). There is a requirement to provide objective data to underpin decisions taken by all stakeholders related to the potential long-term viability and risks of subsurface storage sites and technology.

Remote sensing, integrated with local in-situ measurements, may offer one way to efficiently monitor storage and assess impacts over wide areas (e.g. Pickles and Cover, 2004). To date, including this study, this has involved monitoring the effects on

vegetation of locally elevated CO₂ concentrations in either the atmosphere or in soil gas. Drawbacks of this indirect approach include the seasonal and possibly diurnal changes in plant growth, as well as variable plant stress induced by a variety of unrelated processes (for example, flooding, soil dryness, and agricultural practices).

Here we present results of a remote sensing study of natural CO₂ seeps in central Italy (Bateson et al., 2006), using them as natural analogues of a leaking geological CO₂ storage facility. Since ongoing industrial demonstration projects are unlikely to involve significant leakage in the short term, natural examples of CO₂ seeps provide an alternative opportunity to test and develop monitoring methods. By understanding the behaviour of such natural analogues (Pearce and West, 2006), appropriate monitoring methods can be designed for the geological storage of carbon dioxide, the most important greenhouse gas that contributes to global warming.

As in other studies, this work looks at the indirect effects of CO₂ release on the health and stress level in plants. In order to address problems associated with the temporal variations mentioned above, the same area was surveyed twice, during the spring and autumn, between which crops and natural vegetation varied in growth height, leaf cover and relative stress or vigour. The spring flight was acquired by the NERC Airborne Research and Survey Facility (ARSF) on behalf of BGS on Sunday May 22nd, 2005, while the autumn flight was acquired by OGS on October 28th, 2005 (Vellico, 2005; 2007). Historical air-photos were also investigated to provide additional temporal information on anomaly size, shape, and location, however these results are not reported here.

Interpretation of the collected remote sensing data yielded a series of polygonal areas outlining anomalous responses from one or more of the techniques used. A selection of

these anomalies were subsequently tested on the ground via near-surface gas geochemistry surveys by URS to ascertain if they are the result of deep gas release.

2. Site Description

The test site is located within the Latera Caldera (central Italy; Fig. 1), a volcanic structure that has not been active for over 0.16 Ma but which still maintains a very high geothermal gradient (Bertrami et al., 1984). It is this elevated heat flow that results in the thermo-metamorphic alteration of buried carbonate units and associated production of natural CO₂ and associated trace gases like CH₄, H₂S, and H₂ (Duchi et al., 1992). Although gas pockets have been discovered in deep drilling conducted for geothermal exploration (Bertrami et al., 1984), this capacity has been overwhelmed by the long-term, continual production of large quantities of CO₂. Based on in-situ reservoir conditions this has been estimated to be 2.58×10^8 moles (or 11,352 tonnes) CO₂ yr⁻¹ over 32 km² (Gambardella et al., 2004). The resultant excess gas migrates along the numerous local and regional faults within the caldera and is released to the atmosphere at spatially-restricted points due to channelled flow (Annunziatellis et al., this issue). The gas flux rate from each of these mofetts, gas vents, and bubbling vents is different, and thus the impact on the near-surface environment is also variable. This means that while high-flux points are clearly visible due to their effect on local vegetation (Beaubien et al., this issue), sites with low fluxes are not always apparent. The goal of this research is to see if remote sensing techniques are capable of locating both types of gas release points.

The Latera caldera itself is a flat-floored, elliptical valley that is about 10 x 8 km in size and which trends approximately NE-SW (Fig. 1). The typical Mediterranean

climate, rich volcanic soil, and relatively low population density all contribute to this being an active agricultural area, with grain and corn cultivation and sheep pasturing being the main activities. The limited infrastructure and forested areas, relatively flat topography, and extended areas of homogenous crop types are all advantageous for the application of remote sensing techniques. The valley also has a number of small, active or abandoned kaolinite and sulphur mines which were likely formed by previous hydrothermal activity; these open pit mines are clearly visible in air photographs as completely white areas. A review of the geology of the Latera Caldera can be found in Annunziatellis et al. (this issue).

The total flight area (Fig. 1, area 1) was reduced for this detailed study to a sub-set region having numerous gas venting features (Fig. 1, area 2), along with two smaller areas for illustrating some specific remote sensing results (Fig. 1, areas 3 and 4).

3. Methodologies

3.1. Remote Sensing Datasets.

Multispectral (ATM and CASI) and LIDAR data were collected during the BGS airborne acquisition in May 2005, and hyperspectral (Eagle), digital photography and LIDAR data were acquired during the OGS survey in October 2005. Simultaneous ground-based GPS measurements were obtained during both surveys at an IGM (Istituto Geografico Militare) benchmark (no. 136702) near the town of Farnese.

3.1.1. Airborne Thematic Mapper (ATM) Data

The Daedalus 1268 ATM is a passive multispectral system. It images 11 bands of spectral data, covering the visible, near infrared, short wave infrared and thermal

infrared regions of the electromagnetic spectrum. The resolution of the ATM data depends on the flying height; in this case data were acquired at a resolution of 2.5 meters.

3.1.2. Compact Airborne Spectrographic Imager (CASI 2)

The CASI 2 sensor has maximum of 18 programmable bands. For the purpose of this study, 15 bands were specified throughout the visible and infrared which could be used to calculate vegetation stress (Table 1). The CASI 2 data were acquired at a resolution of 2 meters.

3.1.3. Hyperspectral scanner (Eagle)

An AISA Eagle 1K hyperspectral pushbroom scanning system was used to acquire data in 63 bands between 402.35 and 989.09 nm (Visible Near Infrared region), as reported in Table 2. Images were processed to obtain a 2m resolution.

3.1.4. Light Detection And Ranging (LIDAR)

LIDAR is an active technique that measures distance via the two-way travel time of a pulse of near infrared light energy ($\lambda=1064$ nm) emitted at variable frequencies (33, 50, 70 or 100 kHz). Two different sensors were flown. The Optech ALTM 3033, used during the May flight, records 33,000 observations per second, collects first return, last return, and intensity data, and had an absolute RMS accuracy of ± 15 cm at the chosen flight altitude. The similar Optech ALTM 3100, used during the October flight, is able to record four different returns, and thus the detail of the survey area is even more accurate.

3.1.5. Digital Camera.

A Rollei 6008 db45 digital camera with a resolution of 4080 x 5440 pixels and a pixel spacing of 9 μm was used to obtain high quality colour photographs. The resolution of each orthoimage is approximately 20-25 cm.

3.2. *Remote Sensing Data Processing*

Pre-processing of the data was conducted to verify pixel values and to ensure that the pixels were in the correct geographical space. All data were projected to UTM zone 32 north.

3.2.1. ATM, CASI and Eagle

ATM and CASI data were pre-processed using radiometric calibration algorithms to produce a radiance image, geo-corrected, and then atmospherically corrected for each strip of data using the Internal Average Relative Reflection (IARR) atmospheric correction. The thermal channel of the ATM dataset was also corrected for atmospheric effects.

The Eagle hyperspectral data was first radiometrically corrected by applying the system calibration file to produce a radiance image. The data was then geometrically corrected using the Smooth Best Estimated Trajectory (SBET) to synchronise the acquired images and the helicopter position relative to the ground; ground control points on the orthophotos helped geo-reference the images. Atmospheric correction was then applied to convert radiance data to reflectance data.

The multi / hyper spectral data were used to calculate a series of indices related to plant stress, including: i) a simple ratio of Red (R) / Near Infrared (NIR); ii) Enhanced

Vegetation index; iii) Atmospheric Resistant Vegetation index; iv) Red edge normalised difference; v) Vogelmann red edge index; vi) Red edge position index; vii) Anthocyan reflectance index; and viii) Normalised Difference Vegetation Index (NDVI) (Lillesand et al., 2004). Tests on all indices showed that NDVI gave the greatest distinction between the healthy and stressed vegetation, while still enabling cultural features, such as roads and buildings, to be identified.

NDVI relies on the spectral response of vegetation in the R and NIR regions of the electromagnetic spectrum, as healthy vegetation with high chlorophyll content reflects strongly in the near infrared region and absorbs strongly in the red region. As such the NIR/R ratio of healthy vegetation will be high while that for unhealthy vegetation will be low. This simple ratio can be normalised using the formula:

$$NDVI = \frac{(NIR - R)}{(NIR + R)}$$

Pixels in the resulting image have values between -1 and +1, with +1 indicating the healthiest vegetation. To calculate this index, CASI Bands 12 (780.76nm) and 6 (670.60nm), and Eagle Bands 41 (775.90 nm) and 31 (680.1 nm), were used as the NIR and R bands, respectively. NDVI was computed for each strip individually and the resulting images subsequently mosaiced to cover the study area.

Images of the bands corresponding to the maximum vegetation reflection, i.e. the 'red' bands used in the NDVI calculation, were also produced (band 12 for CASI and band 41 for AISA Eagle). Finally CASI bands 6, 3, and 1 acquired in May and AISA Eagle bands 30, 19, and 9 acquired in October were combined in RGB to produce a true colour mosaic for the study area for comparison with the October orthophotos.

3.2.2. LIDAR

Each laser pulse in the LIDAR system is associated with two (Optech ALTM 3033) or four (Optech ALTM 3100) returns or reflections. The first reflection is caused by the surfaces closest to the sensor, such as the tops of trees or buildings, while the last reflection is caused by the furthest surfaces, typically the ground. The additional two reflections given in the ALTM 3100 data help improve the detail of the dataset by better defining features like trees and buildings. The resulting data set can be described as “point clouds”, where each point in a cloud has an easting, northing, height and intensity. These points were first classified and then triangulated to produce shaded relief models with different illumination angles that could be used to highlight linear trends. The intensity of the LIDAR reflection was also visualised both as greyscale and colour images.

3.2.3. Orthophotos

The orthophotos were first colour balanced and then geo-referenced using a calibration file containing information about roll, pitch and heading. The individual photos were then combined in a mosaic that was subsequently cut into 1km squares for ease of viewing and interpretation.

3.3. *Gas Geochemistry*

Gas geochemistry techniques were used to verify which of the observed remote sensing anomalies were due to the leakage of deep CO₂ to the atmosphere. A total of 72 soil gas and gas flux measurements were conducted on a series of points inside and outside about 50% of the defined anomalies. Sampling was performed in July 2006, during the dry season when plant growth is limited and the biological production of CO₂

is low. These points were accurately located ($\pm 3\text{m}$) using a TRIMBLE Recon GPS palmtop loaded with the October 2005 orthophoto and the location of all interpreted anomalies (as polygons). To define populations and anomaly thresholds this gas geochemistry data set was combined with a further 200 samples collected at the same time along a 600m long profile that crossed both gas vents and background areas (site 5 in Annunziatellis et al., this issue), thus giving a complete range of values and conditions.

3.3.1. Soil gas

Individual soil gas samples were collected using a 6.4mm diameter, 1.5m long probe pounded to a depth of about 60-80cm (Ciotoli et al., 1999; Ciotoli et al., 1998). After cleaning the probe of atmospheric air, field analyses were conducted by directly attaching an Infrared gas analyser (Drager X-AM 7000) to the probe and pumping until the measured values stabilised. This instrument is equipped with a 0-100% CO₂ IR sensor and electrochemical sensors for H₂ (0-2000ppm) and H₂S (0-100ppm). Samples were also collected for laboratory analysis by injecting 60ml of soil gas collected from the probe into a previously-evacuated, 25ml stainless-steel container. These samples were first analysed for helium on a mass spectrometer (Varian Leak Detector) and then on two gas chromatographs (Fisons 8000-series) for methane, ethylene, acetylene, ethane, propane, carbon dioxide, nitrogen and oxygen + argon.

3.3.2. CO₂ gas flux

CO₂ flux was measured using the closed-circuit, accumulation-chamber technique (e.g. Hutchinson and Livingston, 2001), which determines the rate of increase of CO₂ concentration in an inverted chamber set on the ground surface. The system applied in

this study consisted of an in-house-developed analysis and control unit. After the removal of surface vegetation, the accumulation chamber was pressed firmly to the ground to ensure a proper seal and then the CO₂ concentration within the chamber was measured every second over a 60-second interval. The slope of the first linear interval of increasing CO₂ concentration (in ppm/sec) was then used, together with the geometry of the system, to calculate the flux rate:

$$\phi \text{ CO}_2 = ((\text{ppm/sec}) * (\text{V/A})) * 169.71$$

where V is the chamber volume (0.00115 m³), A is the chamber surface area (0.0165 m²), and 169.71 is a conversion factor to give values in g m⁻² d⁻¹.

3.3.3. Data processing and statistical treatment

The program Statistica6 (Statsoft, Tulsa USA) was used for all statistical analyses, including normal probability plots (NPP). The standard NPP is constructed by rank ordering the deviations from the mean (residuals) and then using these ranks to compute the z values (i.e., standardized values of the normal distribution) based on the assumption that the data come from a normal distribution. The NPP consists of an x-y plot of the residuals vs z values. If the observed residuals are normally distributed, then all values should fall along a straight line. Deviations from a straight line trend can be used to objectively delineate different populations and anomaly thresholds that may be related to origin, migration pathways, or reaction mechanisms (Sinclair, 1991).

4. Results

Examination of the remote sensing data sets was first concentrated on an area where known gas vents occur, to understand the response of each sensor to deep CO₂-impacted

vegetation. This was conducted in area 3 (Fig. 1), where one particularly-well-defined, spatially-isolated vent (“gas vent A” – GVA) shows a wide range of CO₂ soil gas concentrations and flux rates. This feature has already been studied in detail using different geochemical and geophysical techniques (Beaubien et al., this issue; Lombardi et al., 2006; Pearce, 2004; Pettinelli et al., 2004; Pettinelli et al., 2008) and thus it represents an excellent control site. Once the individual methods were examined an approach was developed to combine the results of the various remote sensing techniques, which was subsequently applied to a larger area in a blind test to define anomalies that may be due to CO₂ venting (area 2, Fig. 1). Finally, a percentage of the remote sensing anomalies defined in area 2 were examined on the ground using near-surface gas geochemistry techniques to verify if these locations show evidence of deep gas migration to the atmosphere.

4.1. Testing sensor response on known vents

4.1.1. Vegetation Indices

As the name implies, the definition of vegetation index anomalies requires that the study area is vegetated. Bare, ploughed fields must be ignored, as must cultural features such as buildings and roads. The shape of the feature also needs to be considered, as gas vents appear to be more circular or elliptical in shape than features caused by ploughing, which tend to be elongated and linear. Having access to a good quality aerial photograph, preferably taken at the same time as the multi / hyperspectral data was found to be necessary to give context to a feature.

As outlined in the methods section, the various vegetation indices (e.g. NDVI, EVI, ARVI) all clearly define GVA, however NDVI was found to best highlight anomalies

while at the same time distinguish man-made infrastructure. Figure 2 shows the CASI NDVI results from May, 2005, with brighter areas highlighting healthier vegetation and darker areas indicating unhealthy or stressed vegetation. Known gas vents are circled and the three strongest are labelled GVA, GVB and GVC. Here the distribution of the stressed vegetation around GVA is clearly indicated. The centre of the feature, where the soil gas is highest, has no vegetation and thus appears black on the image. Surrounding the black area is a halo of slightly lighter pixels as the vegetation gradually becomes less stressed, presumably in response to lower CO₂ values. Beyond this darker halo the pixels have a similar value to the rest of the field, indicating that the vegetation has returned to a normal state of healthiness. GVB and GVC are also well defined in this data set.

Comparisons between the May and October data (not shown) reveal some differences, most of which are due to changes in vegetation cover and environmental conditions. Both NDVI images produce similar results for GVA, however, which is encouraging considering that the vegetation type was different when the two datasets were gathered: 40-50cm high grass in May and ~15cm high clover in October. This implies that NDVI has the potential to define CO₂-related anomalies for different vegetation types.

4.1.2. ATM Thermal

Figure 3 shows the ATM thermal results for the same area as Figure 2; once again GVA is clearly visible. The vent appears brighter than the surroundings, indicating that the ground is warmer. A halo pattern similar to that seen in the NDVI image is also apparent. The fact that the vent areas appear warmer than the surroundings may be

because: i) the escaping gas is warmer than the surroundings; or ii) the bare-earth of the vent (caused by the high CO₂ concentrations) heats up faster than the surrounding vegetation. Although the second explanation is more likely, it should be remembered that the bright anomaly surrounding GVA in Figure 3 is much larger than the non-vegetated core of the vent. Instead, this anomaly encompasses a transitional zone where there is a mix of grasses, die-back, and clover (Beaubien et al., this issue). In any case, these brighter patches on the thermal image do closely correspond to the areas of stressed vegetation on the NDVI image. Note again that GVB and GVC are clearly visible, and that there are also tonal contrasts for some of the lesser vents.

4.1.3. LIDAR Intensity

Two factors control the intensity of the LIDAR return, surface roughness and moisture content. Rough surfaces cause more backscatter leading to a higher recorded intensity, while wetter ground absorbs more LIDAR energy resulting in lower backscattered intensities.

Figure 4a shows the October LIDAR results. In general the field is characterised by high intensity backscattering (red) caused by healthy vegetation (predominantly clover) and dry surface soil caused by normal evapo-transpiration. At the other end of the scale blue shows low backscatter areas, such as smooth roads or ploughed fields with high moisture contents. GVA is clearly visible as a core with low backscatter amplitude surrounded by a halo of intermediate reflectivity ground that corresponds with that observed in the NDVI and ATM thermal data. The low backscatter core is likely due to moist, smooth, bare soil, while the halo delineates the zone of stressed vegetation

around the core. This dataset, perhaps best of all, also defines the other known vents in this field.

The LIDAR data collected in May, when grass was dominant, has a more variable mid-range backscatter intensity (Fig. 4b) compared to the October results. The non-vegetated core of GVA is still visible in these results, although the surrounding halo is much less pronounced and its edges less defined. Essentially none of the other vents are visible. The variability observed in the background areas could be caused by the blowing flat of the tall grass in some places, because a lower intensity would be recorded for these flattened areas compared to areas unaffected by the wind.

4.1.4. Vegetation Reflectance

Maps were also constructed using data from the region of the electromagnetic spectrum in which healthy vegetation reflects the most energy. For this work, CASI band 12 (780.76nm) and Eagle band 41 (775.90nm) were chosen. Carefully stretched greyscale images of these bands (not shown) highlight non-vegetated areas and areas of unhealthy vegetation that look similar to the NDVI image (Fig. 2).

4.1.5. Spectral analysis

The spectral signatures of two pixels, one inside GVA and one in the background area, were analysed to see if there is any difference between the response of healthy and unhealthy vegetation (Fig. 5). This plot shows that the two signatures are essentially the same between 0 and 0.7 μm and that the chlorophyll absorption peaks are clearly visible in both trends. In contrast the reflectance values diverge rapidly after 0.7 μm , becoming lower for the vegetation inside the vent compared to the higher values in the healthy

background vegetation. This low reflectance value is likely related to vegetative stress induced by the presence of high CO₂ concentrations.

4.1.6. True Colour Images.

An examination of true colour images can indicate vegetative stress, which often shows as browner areas within healthy green vegetation. Orthophotos (Fig. 6) and CASI data (bands 6, 3, and 1 displayed in RGB, not shown) were used for these interpretations. The orthophotos were far easier to interpret due to the higher resolution, which also helped give context to possible areas of interest. The air photo in Figure 6 shows GVA with its characteristic non-vegetated core surrounded, primarily to the south, by patchy and unhealthy vegetation (grey-green areas). GVB, GVC, and the diffuse vent north of GVC are also clearly visible due to a brown-green colour.

4.2. *Method testing and verification*

A larger area (area 2, Fig. 1) was subsequently studied as a blind test, whereby anomalies were defined manually on 6 individual data sets based on the responses identified above in area 3. A selection of these anomalies was then measured in the field using gas geochemistry methods. The chosen remote sensing techniques included NDVI-May, NDVI-October, ATM Thermal, Eagle band 41, CASI band 12, and orthophotos. Examples for each method are given in Figure 7 for a subset (area 4) of area 2.

4.2.1. Integration of remote sensing data sets

As the correspondence of multiple anomalies (defined using different methods and possibly measured in different seasons) may indicate an area having stressed or

unhealthy vegetation, overlapping polygons were grouped and assigned a class number according to how many techniques showed an anomaly for that location (i.e. from 1 to 6). With this approach equal weighting was given to each method (dataset), and the areas defined by a larger number of grouped polygons were expected to have an increased likelihood of outlining areas of unhealthy vegetation. However, as stressed vegetation can be caused by a number of different processes, of which the addition of deep CO₂ is only one, ground measurements were needed to verify the cause. The ultimate goal of this approach is therefore to reduce the costs and time of ground monitoring by defining a number of anomalies, some of which would be false positives while the rest would be “all” points where deep CO₂ leakage is occurring. In this context “all CO₂ leaking points” can be defined as those sites where deep gas flux and concentrations are sufficient to have an impact on the surface ecosystem; sites below this threshold would not be visible with the techniques applied in this study.

The results of this grouped polygon approach are given in Figure 8 for area 2, with each class being assigned a different polygon fill colour to help visually rank the importance of the different anomalies. This figure highlights a number of known vents, however it also indicates the potential occurrence of other vents in areas that had not been previously examined. The results of this blind test were subsequently tested via direct gas geochemistry measurements to determine if these anomalies are due to CO₂ leakage at surface, or to other, unrelated, processes.

4.2.2. Soil gas verification

Since CO₂ is also produced via near-surface biological processes a total of four parameters were measured to ascertain if a given site is a leakage point for deep

endogenic gas. These parameters were CO₂ flux, and soil gas concentrations of CO₂, He, and CH₄. Helium was chosen because it is stable, relatively insoluble, mobile, not involved in biological reactions, and has a deep origin. Methane was examined because concentrations up to 1500 ppm are associated with the deep CO₂ and because it is biologically consumed in aerobic soils (thus values above atmospheric concentrations are typically due to a deep source). See Annunziatellis et al. (this issue) for a discussion of the spatial relationships between these four parameters.

Normal Probability Plots were created and changes in slope were used to define 3 to 4 populations for each parameter (Table 3); these populations are likely linked to different factors related to the origin, production, or consumption of that gas. Each population was assigned a weighting factor, from 1 for background values up to 3 (or 4) for highly anomalous values (Table 3). Thus, each sample was associated with 4 weighting factors, one for each parameter, which were summed to objectively characterise that location: i) 4: definitely not a gas vent (i.e. all four parameters at background levels); 5-6: probably not a gas vent; 7-8: probably a gas vent; and 9-13: definitely a gas vent.

These results were compared with the class value of each tested polygon, with the expectation being that the higher classes would have a higher percentage of gas vents. An examination of Figure 9a, however, shows that success rate does not increase with class number. Instead, combined classes 1 and 2 have a higher success rate (almost 60%) than class 6 (50%), whereas none of the class 5 polygons were considered gas vents. This result implies that giving an equal weight to each of the six applied techniques may not be the best approach, because although all methods may highlight

stressed vegetation, some may be more adept at recognising stress that is due to elevated CO₂.

In order to address this issue the success rate of each individual method was examined. Figure 9b shows how most methods (except Eagle band 41) successfully located between 9 and 11 gas vents (i.e. probably plus definitely gas vents), but that the number of false positives varied significantly. In particular, NDVI October and the orthophoto results gave the highest success rates (about 47% and 42%, respectively) while Eagle band 41 gave the lowest (about 30%). The results and spatial distribution of all measured polygons are given in Figure 10.

5. Discussion

5.1. Minimum fluxes that can be recognised using remote sensing methods.

Examination of all remote-sensing-defined gas vents shows an extremely wide range in CO₂ flux (10 to 3000 g m⁻² d⁻¹) and soil gas CO₂ concentration (5.6 to 97.2%) values. Based on a plot of this data (Fig. 11) a rough threshold of about 60 g m⁻² d⁻¹ can be given as the minimum CO₂ flux rate recognised using the chosen remote sensing techniques during this sampling season and at this site. This value represents the upper limit of class 2 for CO₂ flux (Table 3), implying that classes 1 and 2 may represent biological “background” processes while classes 3 and 4 represent deep flux. It must be remembered, however, that soil gas sampling was conducted during the dry season when biological production of CO₂ is low (to improve soil gas sampling and recognition of a deep gas signal), whereas the remote sensing flights were performed during the spring and fall growing seasons (to improve the potential to observe plant stress). Based on experience at the site it is possible that near-surface biological flux rates (i.e. the

background populations) would have been higher during the flight periods, and thus the remote sensing techniques may have defined some gas vents whose flux rates were actually in the range of the natural background level of that season. This is a promising result considering that it is the low flux points that will be hardest to locate, and implies that some plant-stress hyperspectral measurements (such as NDVI) may have the potential to highlight stress induced by CO₂. In any case, site specific measurements need to be made for each monitoring program, as overall background distributions will depend upon the local soil, growing conditions, land use practices, and climate.

In addition to considering the previously-unknown, low-flux gas vents that were located with the remote sensing techniques it is also necessary to understand if any known gas vents were not located during this test. Based on the results of an older reconnaissance survey conducted in July 2000 (soil gas only) this remote sensing survey missed at least 5 likely gas vents in the study area (stars in Fig. 10, each representing soil gas samples having more than 10% CO₂). Research is underway to study these points to understand why they were not located (such as low CO₂ flux, bare earth, plant type, in shadow, etc.)

5.2. Most appropriate remote sensing method.

By examining only those anomalies that were verified by soil gas analyses as being gas vents, tentative conclusions can be drawn on which methods work best for specific conditions. Where no vegetation exists, for example in ploughed fields, measures of chlorophyll contents (i.e. NDVI) are clearly inappropriate. However both thermal (ATM) and CASI (B12) data did successfully identify some verified gas vents in areas that were non-vegetated in October and May. However, considering that these

techniques also identified anomalies in non-vegetated areas that turned out not to be gas vents, these methods need to be improved.

In fields containing crops, NDVI seems to consistently identify the most verified gas vents, although as outlined above the number of false positives changes from a relatively low value of 10 in the NDVI October data to a much higher value of 17 in the NDVI May results (Fig. 9b). Research is on-going to understand if spectral signature analysis of defined anomalies may aid in increasing the overall success rate of the NDVI technique via the filtering out of false positives.

In the flatter base of the caldera a combination of most of the techniques (NDVI, thermal, CASI and orthophotos) provided the best chance to correctly identify a gas vent. Of the 15 confirmed gas vents identified by remote sensing techniques, 11 were identified by the May NDVI, 10 by CASI and thermal techniques and 9 by October NDVI and orthophoto techniques.

5.3. Seasonal and diurnal influences on data acquisition.

Different techniques will be more appropriate in different seasons according to the types of vegetation present. In an actively farmed area such as this, fields will contain crops at different stages of growth at different times of year. The best season will therefore be very site specific and depend on cultivation practices, types of vegetation, and seasonal weather variations, all of which affect crop growth. In addition, the time of day is also critical. For example, thermal data should be acquired before sunrise and in mid-winter, to prevent the sun's energy heating up the earth's surface and potentially masking thermal variations due to venting gas. In contrast, orthophoto and hyperspectral

data should be acquired as close to midday as possible to reduce artefacts and loss of data caused by shadows.

Within the data acquired here, only the NDVI measurements allow direct comparisons between the two datasets collected during different seasons. The May NDVI data identified 10 verified gas vents whereas the October NDVI data identified 8 gas vents, of which 6 were identified in both datasets. Further interpretation is required to determine if this is due to variable plant responses at different times of year, changing crops, or a lack of vegetation altogether in some areas.

5.4. Where can remote sensing be applied?

Many different remote sensing techniques identified anomalies (Fig. 7) on the hill slopes of area 4 (Fig. 1), anomalies that gas geochemistry results eventually showed were not due to deep gas migration. The reasons for this are unclear, however if an explanation could be found that would filter out these false positives the overall success rate of the remote sensing test would increase from 39% to over 50%. While it is to be fully expected that false positive results will be obtained (there are many factors that could cause stress in plants), Figure 10 shows that the greatest success rates were on the relatively-flat caldera floor. In addition, no anomalies were identified in wooded areas. This implies that reasonably flat land with low relief and short, homogeneous or sparse vegetation would be terrain best suited to remote sensing for detection of CO₂ leaks. That said, it is unknown if gas vents occur in the hill slopes or wooded areas, as they represent zones with different geological units and structures.

5.5. *Limitations.*

One significant limitation of the described approach is that the area is a natural system that has developed over geological time, and thus there is the potential that the seepage sites are in a steady state and that the natural vegetation (but not the cultivated plants) may have adapted or substituted species to cope with the higher CO₂ concentrations. Clearly this would not be the case for a new seep from a CO₂ geological storage site, where both remote sensing and gas geochemistry surveys could be conducted before injection begins to define baseline conditions. If possible repeat surveys during different seasons would be of great use to define pre-existing anomalies (caused by other factors) and to establish natural variations, which could be used to help remove potential false positive results in subsequent surveys.

Instrumental limitations arise from the indirect nature of locating CO₂ leaks by using methods that measure vegetative stress, as plant health is affected by many factors that are unrelated to CO₂ concentrations. Techniques such as NDVI are particularly prone to this problem, however the application of spectral signature analysis (Fig. 5) has the potential to greatly improve this approach. More research is required, however, to understand the cause of the spectral difference and if it is observed in different plant species (or even caused by the occurrence of a different plant species in the area of elevated CO₂ concentrations). In fact, too little is known regarding the effect of CO₂ on different plant species.

Finally another limitation is the amount of time required to manually interpret the various datasets, particularly if a large area is covered and many instruments are flown. Future work should examine the potential for automating part of the site selection

process, even if a qualified technician who has, preferably, visited the site is indispensable for proper interpretation.

6. Conclusions

Results of this preliminary application of remote sensing techniques to the search for gas release points has shown that this approach has potential as a regional screening technique to choose anomalous sites for more detailed, ground-based study. Subsequent detailed site monitoring must include near-surface gas geochemical measurements to ascertain whether the anomaly is caused by deep CO₂ leakage or by some other, unrelated process.

Hyperspectral remote sensing techniques can detect plant stress and, in some cases, this was subsequently verified as being attributable to deep gas venting. Although the major gas being released is CO₂, the presence of H₂S in the strongest gas vents remains a complicating factor which must be addressed in future research. These techniques also identified many anomalies that could not be attributed to gas vents and thus future work should focus on reducing the number of false positive results through the application of innovative techniques such as spectral signature analysis. False positives can also be reduced at an actual CO₂ geological storage site via the careful acquisition of baseline data prior to injection. Finally, thermal data were able to detect some anomalies in non-vegetated areas (ploughed fields), while high quality orthophotos proved invaluable in aiding interpretation of other datasets.

The most appropriate season for data acquisition is discussed for each technique; clearly measures of vegetation stress can only be effective when plants are in leaf. In developing a monitoring plan for a storage site, careful consideration should be given to

the land management and cultivation practices, together with the seasonal variations within the region of interest.

Future work planned at the Latera site to address some of the questions raised by this research include: i) combined interpretation of remote sensing and ecosystem parameters to better understand how different plant species respond to different CO₂ levels; ii) a more detailed examination of the data to address how vegetation response changes with season; and iii) direct detection of elevated atmospheric CO₂ above natural seeps by airborne remote sensing techniques (flown during the fall of 2007, with data interpretation scheduled to begin in 2008). If direct detection of CO₂ proves successful, this could help to better focus ground-based verification and reduce the number of false positive measurements.

7. Acknowledgements

The present work was conducted within the framework of CO₂GeoNet, a European Community funded “Network of Excellence” dedicated to the study of all aspects of geological CO₂ storage; funding from the EC and from each of the author’s institutions is gratefully acknowledged. The authors would like to thank colleagues at NERC ARSF for their fundamental contribution to the success of this research: Carl Joseph, David Davies, and David Cobby. This paper is published with the permission of the Executive Director, BGS (NERC). Finally we would like to thank the anonymous reviewers of our article for their useful comments and suggestions.

8. References

- Annunziatellis, A., Beaubien, S.E., Bigi, S., Ciotoli, G., Coltella, M., Lombardi, S., this issue. Gas migration along fault systems in the Latera natural analogue (central Italy): implications for CO₂ geological storage. *Int. J. Greenhouse Gas Control*.
- Bateson, L., Vellico, M., Beaubien, S.E., Annunziatellis, A., Ciotoli, G., 2006. Testing remote sensing monitoring technologies for potential CO₂ leaks. CO₂GeoNet Internal Report. pp 57.
- Beaubien, S.E., Ciotoli, G., Coombs, P., Dictor, M.C., Krüger, M., Lombardi, S., Pearce, J.M., West, J.M., this issue. The impact of a naturally-occurring CO₂ gas vent on the shallow ecosystem and soil chemistry of a Mediterranean pasture (Latera, Italy). *Int. J. Greenhouse Gas Control*.
- Bertrami, R., Cameli, G.H., Lovari, F., Rossi, U., 1984. Discovery of Latera geothermal field: problems of the exploration and research. Seminar on Utilization of Geothermal Energy for Electric Power Production and Space Heating, Florence, May 14-17, 1984.
- Ciotoli, G., Etiope, G., Guerra, M., Lombardi, S., 1999. The detection of concealed faults in the Ofanto Basin using the correlation between soil-gas fracture surveys. *Tectonophysics*, 301, 321-332.
- Ciotoli, G., Guerra, M., Lombardi, S., Vittori, E., 1998. Soil gas survey for tracing seismogenic faults: A case study in the Fucino basin, central Italy. *Journal of Geophysical Research*, 103(B10), 23,781-23,794.
- Duchi, V., Minissale, A., Paolieri, M., Prati, F., Valori, A., 1992. Chemical relationship between discharging fluids in the Siena-Radiocfani Graben and the deep fluids produced by the geothermal fields of Mt Amiata, Torre Alfina and Latera. *Geothermics*, 21(3), 401-413.
- Gambardella, B., Cardellini, C., Chiodini, G., Frondini, F., Marini, L., Ottonello, G., Vetushi Zuccolini, M., 2004. Fluxes of deep CO₂ in the volcanic areas of central-southern Italy. *Journal of Volcanology and Geothermal Research*, 136, 31-52.
- Hepple, R.P., Benson, S.M., 2005. Geologic storage of carbon dioxide as a climate change mitigation strategy: performance requirements and the implications of surface seepage. *Environmental Geology*, 47(4), 576-585.
- Hutchinson, G.L., Livingston, G.P., 2001. Vents and seals in non-steady-state chambers used for measuring gas exchange between soil and the atmosphere. *Eur. J. Soil Sci.*, 52, 675-682.
- Lewicki, J.L., Hilley, G.E., Oldenburg, C.M., 2005. An improved strategy to detect CO₂ leakage for verification of geologic carbon sequestration. *Geophysical Research Letters*, 32, doi:10.1029/2005GL024281.
- Lewicki, J.L., Oldenburg, C.M., 2004. Integrated near-surface monitoring and analysis for CO₂ storage verification. Abstracts of Papers of the American Chemical Society, 227, U1099-U1099.

- Lillesand, T.M., Kiefer, R.W., Chipman, J.W., 2004. Remote sensing and image interpretation. John Wiley & Sons, New York.
- Lombardi, S., Annunziatellis, A., Ciotoli, G., Beaubien, S.E., 2006. Near surface gas geochemistry techniques to assess and monitor CO₂ geological sequestration sites. In: Lombardi, S., Altunina, L.K., Beaubien, S.E. (Eds.), *Advances in the Geological Storage of Carbon Dioxide*. NATO Science Series, IV. Earth and Environmental Sciences. vol 65. Springer, pp. 141-156.
- Oldenburg, C.M., Lewicki, J.L., 2006. On leakage and seepage of CO₂ from geologic storage sites into surface water. *Environmental Geology*, 50(5), 691-705.
- Pearce, J.M. (Ed.), 2004. Natural analogues for the geological storage of CO₂. Final report of the Nascent project. British Geological Survey Technical Report, 122 pp.
- Pearce, J.M., West, J.M., 2006. Study of potential impacts of leaks from onshore CO₂ storage projects on terrestrial ecosystems. British Geological Survey report.
- Pettinelli, E., Passaretta, A., Cereti, A., Menghini, A., Annunziatellis, A., Ciotoli, G., Beaubien, S.E., Lombardi, S., 2004. GPR and EM31 investigations on an active CO₂ gas vent. Tenth International Conference on Ground Penetrating Radar, Delft, The Netherlands, June 21-24, 2004.
- Pettinelli, E., Beaubien, S.E., Lombardi, S., and Annan, A.P., 2008. GPR, TDR, and geochemistry measurements above an active gas vent to study near-surface gas-migration pathways. *Geophysics*, 73(1), doi: 10.1190/1.2815991.
- Pickles, W., Cover, W., 2004. Hyperspectral geobotanical remote sensing for CO₂ storage monitoring. In: Benson, S.M. (Ed.), *Carbon dioxide capture for storage in deep geologic formations*. Elsevier Ltd, Oxford, 2, 1045-1070.
- Sinclair, A.J., 1991. A fundamental approach to threshold estimation in exploration geochemistry: probability plots revisited. *J. Geochem. Explor*, 41, 1-22.
- Vellico, M., 2005. Remote sensing techniques applied to CO₂ natural analogues studies. Annual report 2005, OGS - Geophysics of the Lithosphere Department
- Vellico, M., 2007. Metodologia iperspettrale e laser - scanning per l'individuazione di fuoriuscite naturali di CO₂: la caldera di Latera, University of Trieste, Trieste, Italy.
- West, J.M., Pearce, J.M., Bentham, M., Maul, P., 2005. Environmental issues and the geological storage of CO₂. *European Environment*, 15, 250-259.

Captions

Figure 1: Schematic map of the Latera caldera, central Italy (inset). The 4 areas outlined represent: 1) total flight area for the remote sensing study; 2) subset area chosen for blind test; 3) subset area with known gas vents, for testing the response of the remote sensing methods; and 4) subset area where some detailed results are shown.

Figure 2. CASI NDVI results for area 3 (Fig. 1). The grey-scale ranges from +1 for healthy vegetation (white) to -1 for unhealthy vegetation (black). Known gas vents are circled, and the three strongest are labelled as gas vents A, B, and C.

Figure 3: ATM Thermal data for area 3 (Fig. 1). The grey-scale ranges from warmer (white) to cooler (black) ground. Known gas vents are circled, and the three strongest are labelled as gas vents A, B, and C.

Figure 4: a) OGS LIDAR intensity data (ground class) for area 3 (Fig. 1). The intensity is displayed as an elevation: dark blue corresponds to no intensity data (where trees and buildings have been removed) whereas red is the highest intensity. b) BGS LIDAR last return intensity data for area 3. Known gas vents are circled, and the three strongest are labelled as gas vents A, B, and C.

Figure 5. Spectral signatures of healthy (background) and unhealthy (from GVA) vegetation.

Figure 6: Orthophoto of area 3 (Fig. 1), clearly showing the form and extent of GVA via its effect on vegetation cover and colour.

Figure 7. Trial interpretations of six datasets for a smaller region (area 4, Fig. 1), located to the southwest of area 3: a) NDVI May; b) NDVI October; c) CASI band 12; d) Eagle band 41; e) ATM thermal; and f) orthophoto.

Figure 8. Grouped interpretations for subset area 2. Polygon colours correspond to the number of datasets (methods) that showed an anomaly within that polygon (i.e., classes 1 to 6). Numerous polygons with the value of 1 are not displayed to avoid cluttering the map. Note the location of area 3 in the centre of the figure.

Figure 9. Percentage and absolute numbers (labels) of anomalies defined as being gas vents or not based on near-surface gas geochemistry measurements. Results are presented based on the remote sensing class system (a) and the individual techniques (b).

Figure 10. Map showing the distribution of verified gas vents, based on gas geochemistry measurements of remote-sensing-defined anomalies.

Figure 11. Plot of the soil gas CO₂ concentrations and CO₂ flux values for the 15 remote-sensing-defined gas vents. Note the one sample has 55% CO₂ but only 10 g m⁻² d⁻¹ CO₂ flux, implying an error in the CO₂ flux measurement.

Table 1. List of the acquired CASI 2 bands.

Table 2. List of the acquired AISA Eagle 1K bands.

Table 3. Statistically-defined populations (ranges) for the considered gas geochemistry parameters, along with the weighting factor given for each.

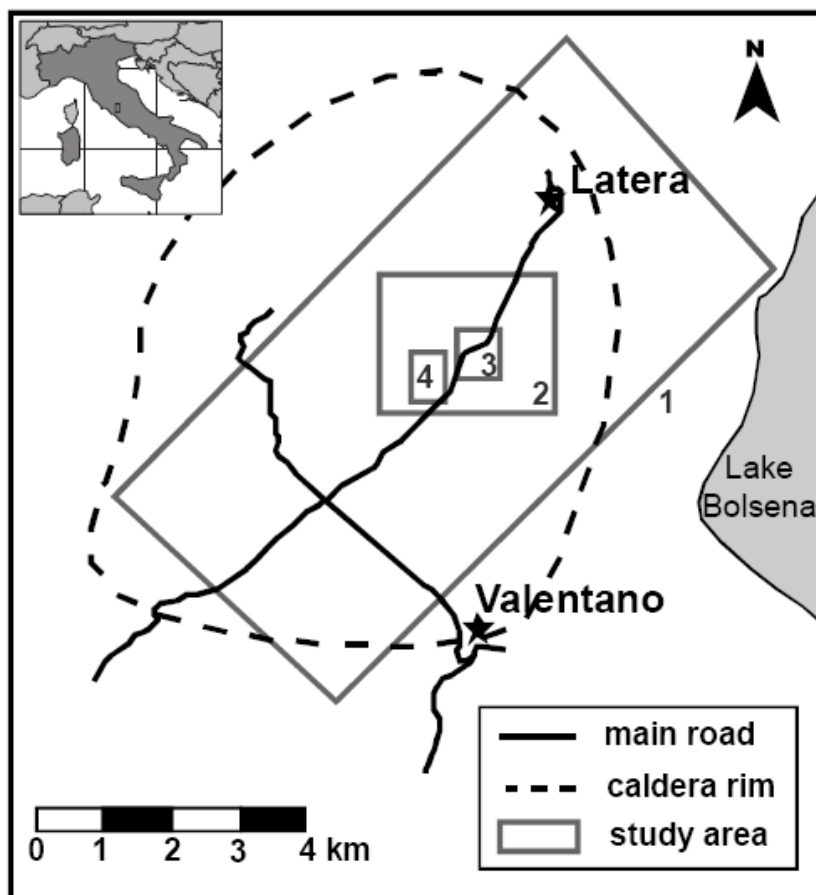


Figure 1



Figure 2



Figure 3

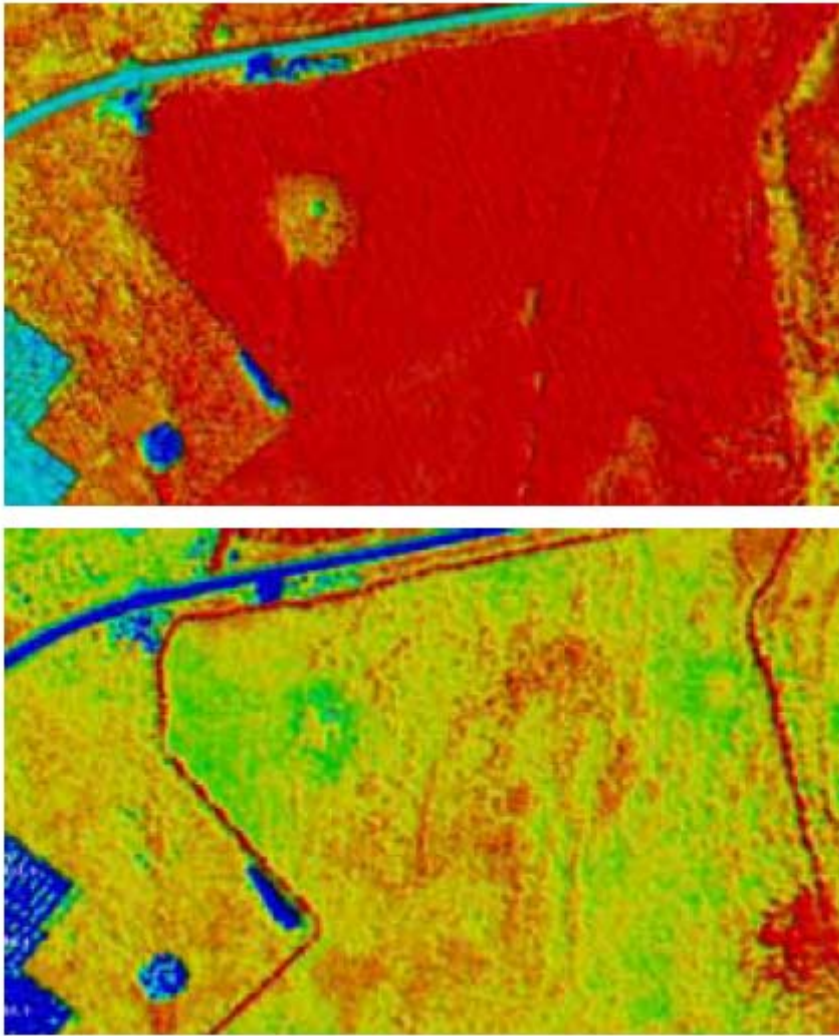


Figure 4

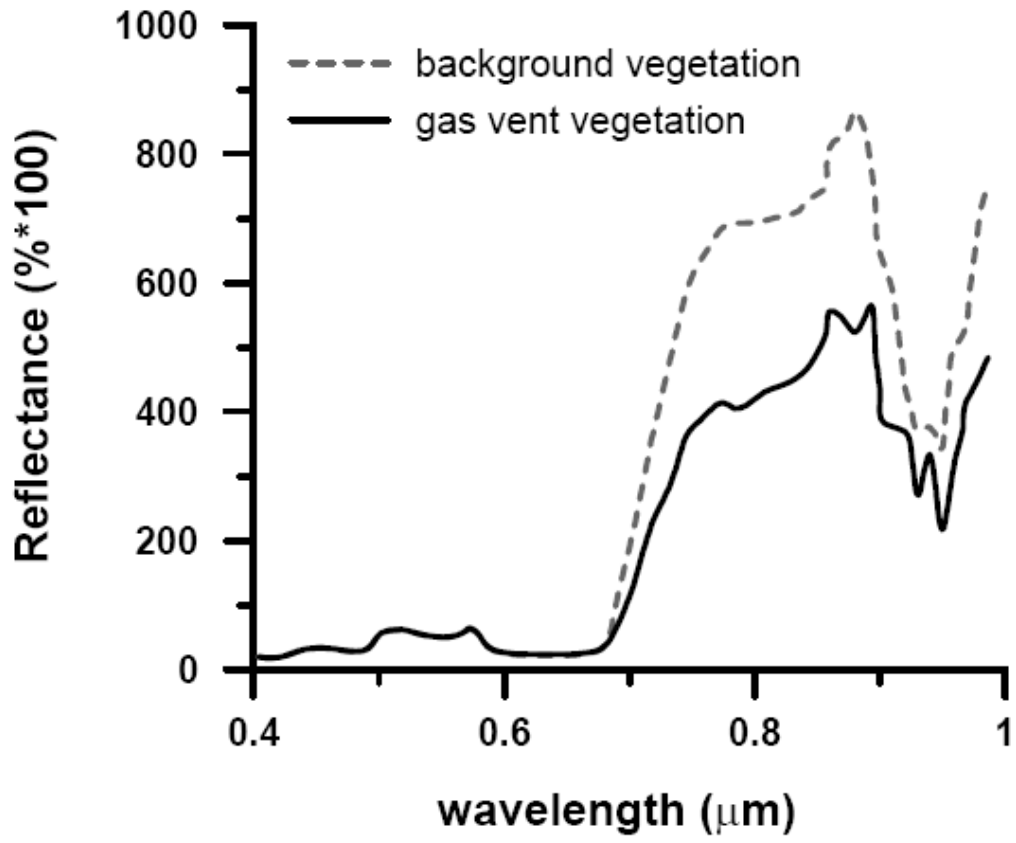
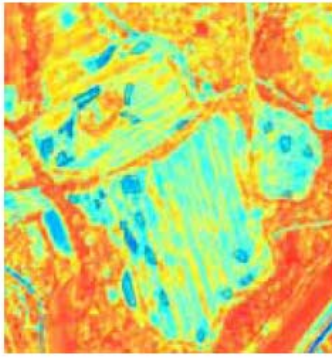


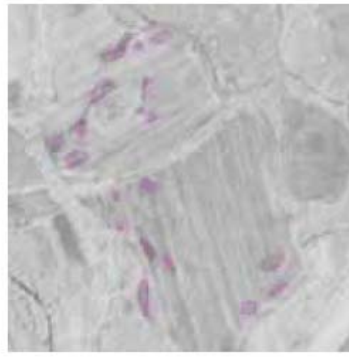
Figure 5



Figure 6



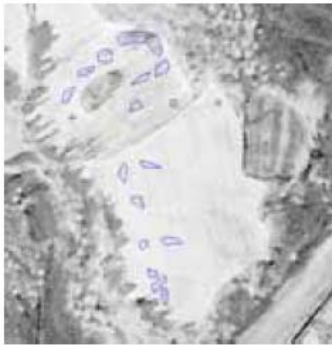
May NDVI



May CASI band 12



May ATM Thermal



October NDVI



October Eagle band 41



October orthophoto

Figure 7

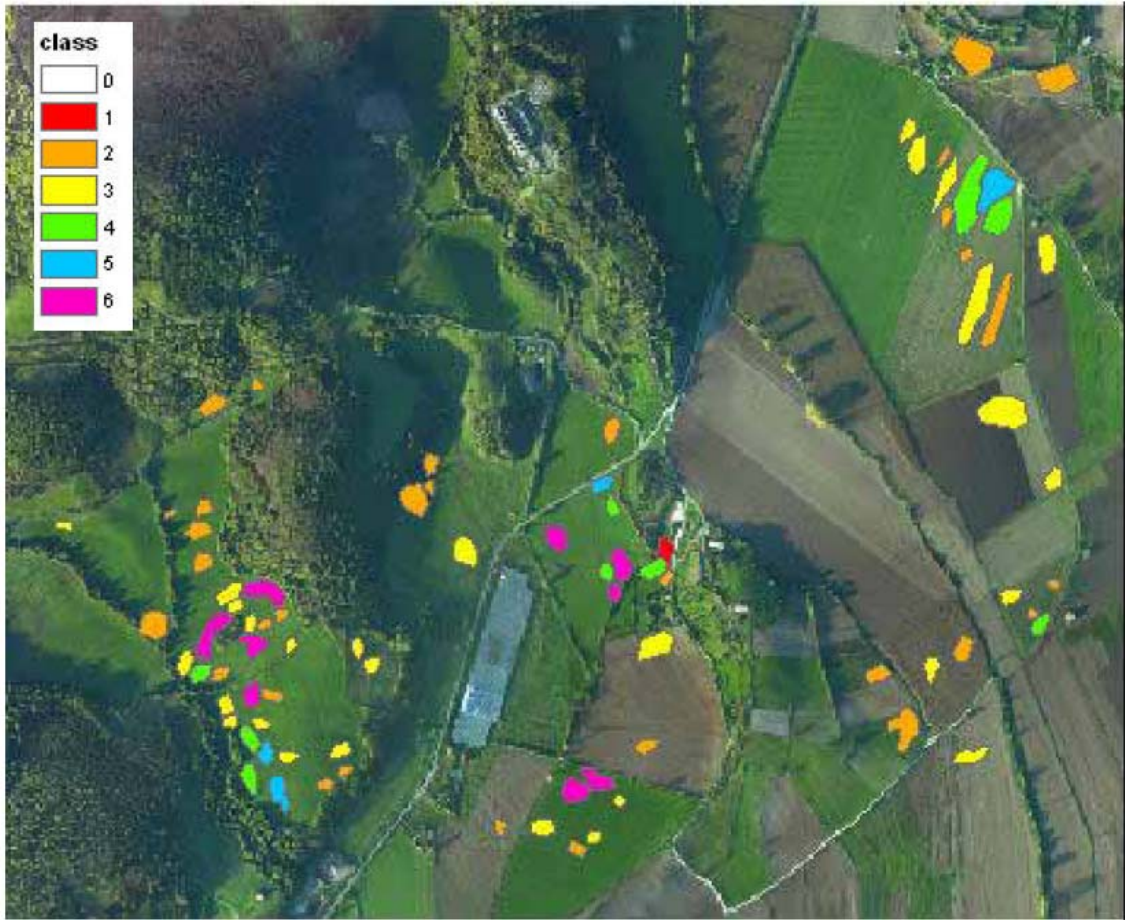


Figure 8

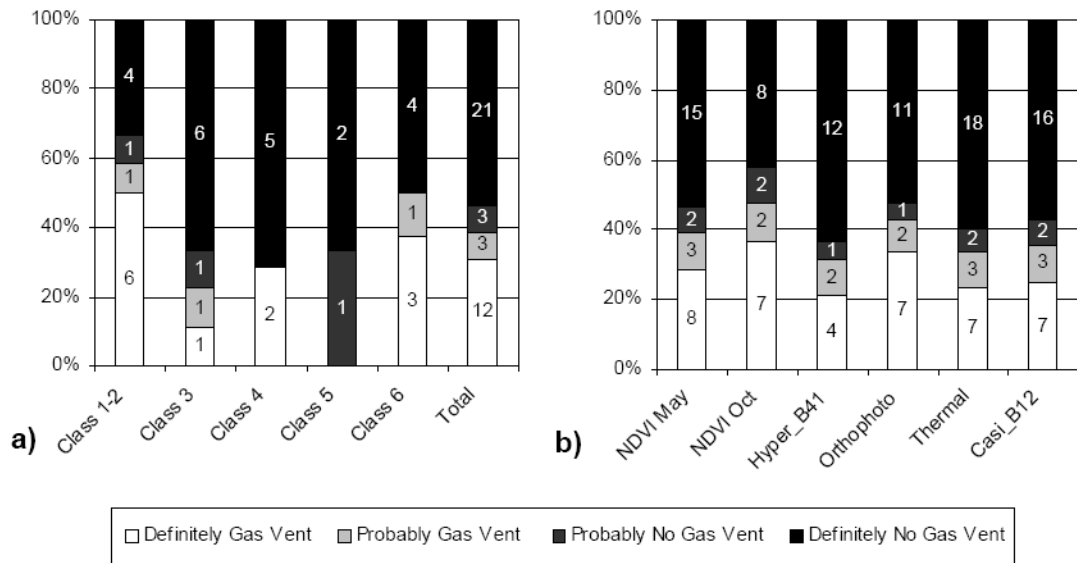


Figure 9.

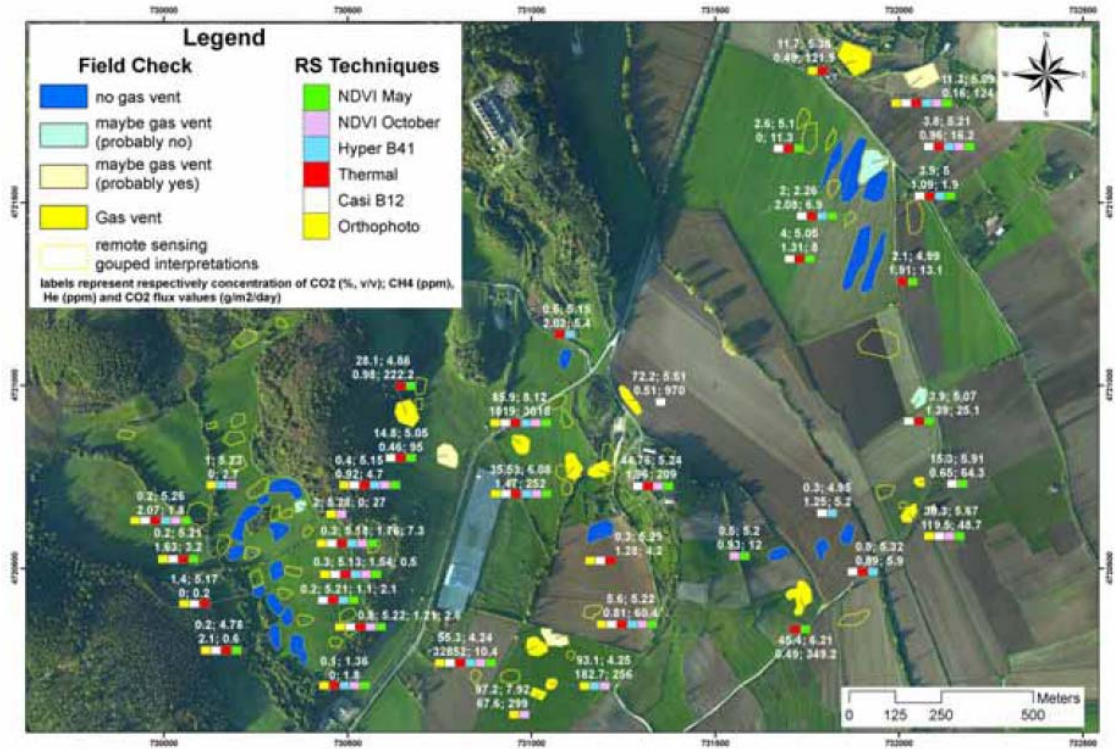


Figure 10

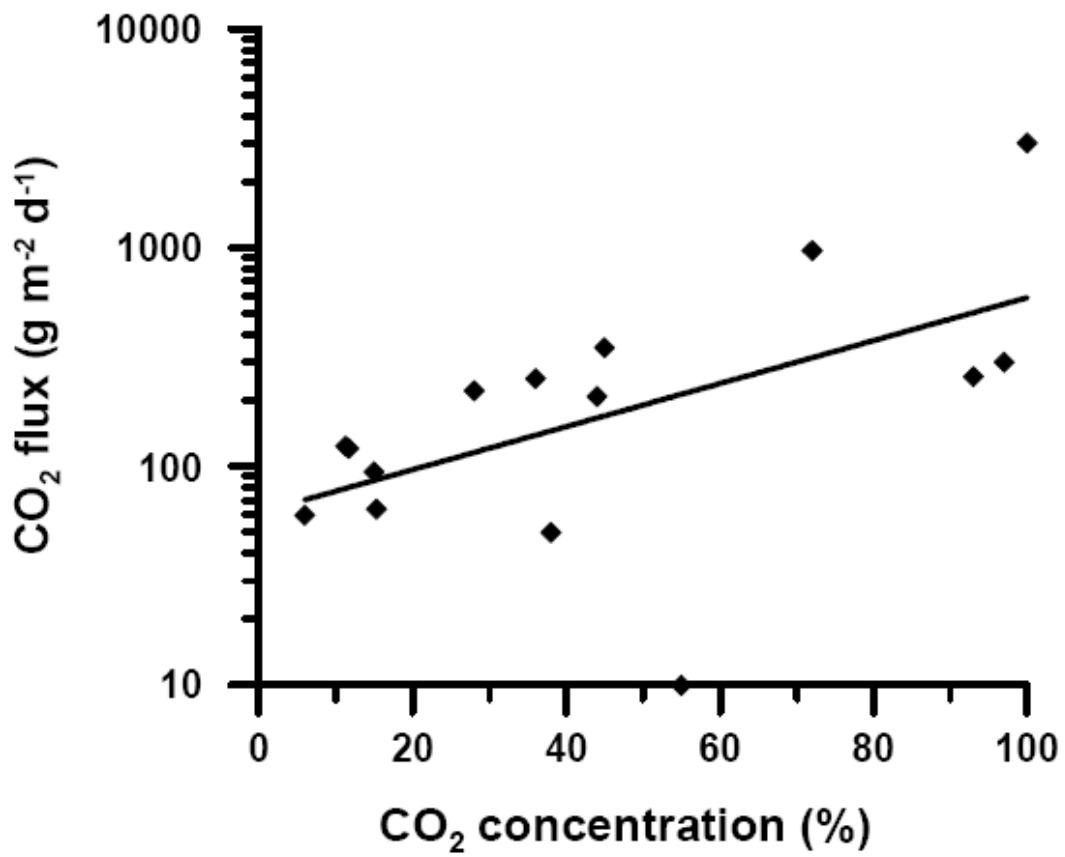


Figure 11

Band Number	Centre Wavelength (nm)
1	449.61
2	489.82
3	551.92
4	907.78
5	650.57
6	670.60
7	701.17
8	710.74
9	741.39
10	750.03
11	762.50
12	780.76
13	820.20
14	864.54
15	939.86

Table 1

Band Number	Centre Wavelength (nm)						
1	402.35	17	547.46	33	699.16	49	853.44
2	411.14	18	556.85	34	708.70	50	863.12
3	419.93	19	566.24	35	718.24	51	872.80
4	428.72	20	575.65	36	727.78	52	882.47
5	437.60	21	585.12	37	737.32	53	892.15
6	446.73	22	594.63	38	746.87	54	901.83
7	455.89	23	604.13	39	756.51	55	911.51
8	465.04	24	613.63	40	766.21	56	921.21
9	474.19	25	623.13	41	775.90	57	930.90
10	483.34	26	632.64	42	785.60	58	940.60
11	492.49	27	642.14	43	795.30	59	950.29
12	501.65	28	651.64	44	805.00	60	959.99
13	510.80	29	661.14	45	814.70	61	969.69
14	519.95	30	670.64	46	824.40	62	979.39
15	529.10	31	680.15	47	834.08	63	989.09
16	538.26	32	689.65	48	843.76		

Table 2

	units	class 1	class 2	class 3	class 4
CO₂ flux	g/m ² /d	0 - 16 (1)	16 - 60 (2)	60 - 300 (3)	300 - 1,500 (4)
CO₂	%	0 - 4 (1)	4 - 16 (2)	16 - 100 (3)	
CH₄	%	0 - 2.2 (1)	2.2 - 500 (2)	500 - 32,000 (3)	
He	%	0 - 5.35 (1)	5.35 - 6.1 (2)	6.1 - 9.2 (3)	

Table 3